BJPS

Brazilian Journal of
Pharmaceutical Sciences

http://dx.doi.org/10.1590/s2175-97902025e24302

Article

Physiologically-based pharmacokinetic modeling of enantioselective hydroxychloroquine kinetics and impact of genetic polymorphisms

Gabriella de Souza Gomes Ribeiro[1], Leandro Francisco Pippa[2], Fernanda de Lima Moreira[3], Natália Valadares de Moraes[4*]

[1]São Paulo State University, Araraquara, Brazil, [2,4]Center for Pharmacometrics & Systems Pharmacology, University of Florida, USA, [3]Federal University of Rio de Janeiro, School of Pharmacy, Rio de Janeiro, Brazil

Hydroxychloroquine (HCQ) is a chiral drug used to treat malaria and inflammatory diseases, available as a racemic mixture of R– and S–HCQ. This work aimed to build physiologically-based pharmacokinetic (PBPK) models to predict the pharmacokinetics (PK) of R– and S–HCQ and assess the impact of major genetic polymorphisms on PK. Whole-body PBPK models accounting for first-order absorption, Rodgers and Rowland distribution method, and enzyme kinetics data were built for R– and S–HCQ. The models were verified by comparing predicted PK parameters with observed ones, with a mean error within the acceptable range (0.5–2 fold). Simulations covered CYP2D6 normal metabolizer (NM), poor metabolizer (PM), and ultra-rapid metabolizer (UM) phenotypes, as well as CYP2C8 NM and PM phenotypes. The results revealed a 1.1-fold increase in area under the curve blood concentration versus time (AUC) for CYP2D6 PM individuals and a 0.9-fold reduction for UM individuals compared to NM individuals. In addition, simulations with CYP2D6 and CYP2C8 PM phenotype individuals combined with the CYP3A4 inhibitor clarithromycin showed increased AUC for R– and S–HCQ of 2.34 and 2.68, respectively. These PBPK models offer reliable predictions for R– and S–HCQ enantioselective kinetics and shed light on previously unexplored scenarios.

Keywords: Hydroxychloroquine. Enantiomers. PBPK. Gene polymorphisms. Drug interactions.

INTRODUCTION

Hydroxychloroquine (HCQ) sulfate, an analog of chloroquine, has been a safe alternative to treat various conditions since 1955 (Ducharme *et al.*..., 1995). Enantioselective pharmacokinetics has been described with higher systemic exposure of *R*–hydroxychloroquine (*R*–HCQ) in blood than for *S*–hydroxychloroquine (*S*–HCQ) (Ducharme *et al.*..., 1995; McLachlan *et al.*..., 1993). *R*–HCQ shows a higher fraction unbound in plasma (0.63) compared to *S*–HCQ (0.36) (McLachlan *et al.*..., 1993). The cellular uptake of *R*–HCQ in erythrocytes, platelets, lymphocytes, and undifferentiated mononuclear and polymorphonuclear cells is higher than that of *S*–HCQ (Brocks *et al.*..., 1994). Both *R*–HCQ and *S*–HCQ exhibit extensive tissue distribution, primarily due to their accumulation in the acidic environment of lysosomes. This phenomenon accounts for their remarkably prolonged half-lives of 22 and 19 days, respectively (Derendorf, 2020). The hepatic metabolism, catalyzed by various cytochrome P450 (CYP) isoforms, results in the formation of the chiral metabolites desethylchloroquine (DCQ), desethyl-hydroxychloroquine (DHCQ) and bisdesethylcholoquine (BDCQ) (Cardoso, Bonado, 2009). Nevertheless, a comprehensive assessment of the intrinsic clearance disparities between *R*–HCQ and *S*–HCQ remains unexplored.

Gaining insight into the enantioselective kinetic behavior of HCQ is paramount in establishing connections between exposure and response, particularly in malaria prevention and treatment, where *R*–HCQ preferentially distributes to blood cells, its site of action (Ruiz-Irastorza *et*

***Correspondence:** N. V. de Moraes Center for Pharmacometrics and Systems Pharmacology Department of Pharmaceutics, College of Pharmacy University of Florida 6550 Sanger Road Orlando, FL 32827, USA Phone: (407) 3137048 Email: nataliademoraes@ufl.edu https://orcid.org/0000-0002-4389-058X

al..., 2010). While the molecular mechanisms of action of HCQ's efficacy in malaria remain incompletely elucidated, it is established that 4aminoquinolines exhibit potent antiparasitic activity on plasmodia by interfering with hemoglobin degradation. Thus, selective distribution to blood cells and binding to plasma proteins seem to be the main contributors to the different antimalarial responses for *R*- and *S*–HCQ in vivo (Brocks, Mehvar, 2003). Besides the pharmacokinetic information and factors related to interindividual variability, antimalarial drug optimization requires parasite susceptibility and parasite burden assessment to characterize exposure-response relationships (Hughes *et al...,* 2021).

Physiologically based pharmacokinetic (PBPK) modeling has emerged as a valuable approach for comprehensively understanding the sources of variability in drug exposure. Its applications span different phases of drug development, the design of clinical trials, and personalized approaches for special populations (Madabushi *et al...*, 2022). PBPK modeling and simulation approach enables a comprehensive understanding of enantioselectivity in drug disposition since slight differences in the spatial structure between chiral compounds can result in different absorption, distribution, transport, and elimination. Leveraging PBPK modeling and simulation to understand enantioselectivity in the kinetic disposition of HCQ, we aimed to build models for a pair of compounds with identical physicochemical properties, but with different blood/plasma binding properties and kinetic disposition. Given that HCQ is metabolized by CYP2C8, CYP2D6, and CYP3A4, the models were applied to simulate the effect of major gene polymorphism on drug disposition.

MATERIAL AND METHODS

Software

Modeling and simulation were carried out on Simcyp™ PBPK Simulator version 21 (Certara, Princeton, NJ, USA). Essential anatomical and physiological parameters, including tissue-specific blood flow, organ volumes, tissue composition, permeability, and expression of metabolic enzymes, along with their variations based on body weight, sex, and age were integrated from the simulator libraries. Parameter optimization was performed using correlated Monte Carlo simulation. This iterative optimization process fine-tuned the model's parameters to accurately align with observed data.

PBPK model building

The compound-specific parameters, including physicochemical properties (molecular weight, log P, acid dissociation coefficient (pKa)), biological properties such as blood/plasma (B/P ratio) and fraction unbound in plasma, parameters to describe absorption, distribution, and elimination of HCQ enantiomers were incorporated using a stepwise fashion approach (Figure 1). A whole-body PBPK human model was developed for *R*–HCQ and *S*–HCQ, separately (Supplementary material, Table SI). The fraction unbound (Fu) was described in vitro, with values of 0.63 for *R*–HCQ and 0.36 for *S*–HCQ (McLachlan *et al...*, 1994). Due to the high penetration of HCQ in blood cells, clinical studies often report blood concentrations and blood clearance (CL_{blood}) rather than plasma clearance (CL_{plasma}). Therefore, the CL_{plasma} was estimated from the intravenous CL_{blood} (Eq. 1) since pharmacokinetic parameters in plasma are used as input data in the simulator,

$$CL_{plasma} = \frac{CL_{blood}}{B/P} = \frac{CL_{blood}}{1 + H\left(\frac{C_{rbc}}{C_{plasma}} - 1\right)} \qquad \textit{Eq. 1}$$

where B/P describes the blood-to-plasma concentration ratio, and H represents the hematocrit, C_{rbc} is the red blood cell concentration, and C_{plasma} is the plasma concentration (Toutain, Bousquet-Mélou, 2004).

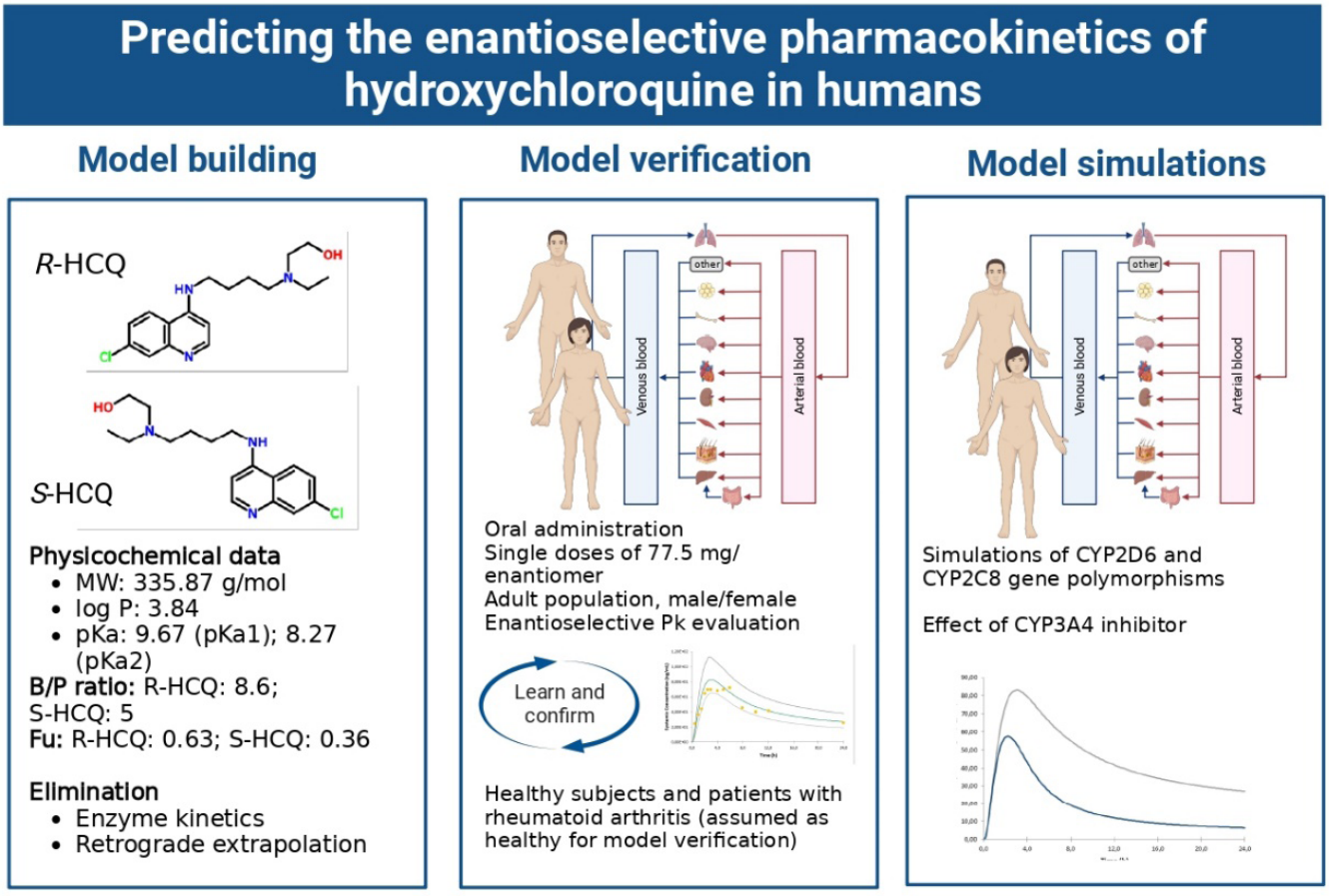

FIGURE 1 - Overall strategy of the PBPK model building, validation, and simulations for *R*–HCQ and *S*–HCQ. Figure prepared with BioRender (https://biorender.com/).

The fraction absorbed (Fa) after oral administration was predicted using the first-order absorption model. Three distribution prediction methods available at Simcyp Simulator were evaluated, including the corrected Poulin and Theil method (method 1), the Rodgers and Rowland method (method 2), and the Rodgers and Rowland method with ion permeability (method 3). The subcellular distribution was also used to capture the lysosomal distribution of HCQ. The major organs contributing to lysosomal sequestration of HCQ were kidneys, lungs, and liver, as these tissues have a larger content of lysosomes (MacIntyre, Cutler, 1998).

Literature data (Ducharme *et al...,* 1995; McLachlan *et al...*, 1994) were reviewed to gather information on renal clearance (CL_{renal}) and CL_{blood} (Supplementary material, Table SII). Based on this, non-renal clearance (CL_{NR}) was calculated, assuming it to be equivalent to hepatic clearance (CL_H) (Equation 2).

$$Cl_{NR} = Cl_H = Cl_T - Cl_R \qquad Eq.\ 2$$

Based on our literature review, there is no enantioselectivity in the plasma hepatic clearance of HCQ. Therefore, in the absence of in vitro metabolism data for each enantiomer, the intrinsic clearances for CYP2C8, CYP2D6, and CYP3A4 were obtained by backward extrapolation based on predicted intrinsic clearance values using the ADMET predictor (Zhang *et al...,* 2021). Additionally, these same enzymes have been described as potential contributors to HCQ metabolism (Tanaka *et al...*, 2004). For the retrograde extrapolation step, the renal CL was defined as 15.4 L/h for *R*–HCQ and 23.0 L/h for *S*–HCQ, as observed in in vivo studies (Tett *et al...,* 1994; Ducharme *et al...*, 1995).

Model verification

The performance of the PBPK model was assessed by comparing the simulated data with in vivo observations from published clinical studies (Ducharme *et al...*, 1995; Midha *et al...*, 1996; McLachlan *et al...*, 1994). Simulations were carried out to verify the model after an intravenous (McLachlan *et al...*, 1994) or single oral dose in healthy volunteers (Ducharme *et al...*, 1995; Midha *et al...*, 1996) and patients with rheumatoid arthritis (McLachlan *et al...*, 1994). Data such as study duration, administered dose, population, number of volunteers, age, and percentage of women are available in Table I. The administered dose in adults, whether orally or intravenously, was 200 mg of HCQ sulfate, corresponding to 155 mg of free base HCQ, or 77.5 mg of each enantiomer. Simulations were further carried out to verify the enantioselectivity of HCQ enantiomers and to evaluate the effects of CYP2D6 and CYP2C8 genetic polymorphisms, as well as to investigate the influence of these polymorphisms in the presence of a CYP3A4 inhibitor drug. The observed blood concentration profiles of *R*–HCQ and *S*–HCQ were extracted using the WebPlotDigitalizer tool (https://automeris.io/WebPlotDigitizer/).

TABLE I - Clinical study data used to verify the *R*-HCQ and *S*-HCQ PBPK models

Compound/ administration	Dose (mg)	Population	Dosage regimen	n	Years	Duration of the study	% of women	Ref.
Oral *R*-HCQ	77.5	healthy volunteer	single	24	20–36	168 h	0	2
Oral *R*-HCQ	77.5	healthy volunteer	single	72	19–50	77 days	0	3
IV *R*-HCQ	77.5	patient with rheumatoid arthritis	single	9	50±16	32 h	77.7	1
Oral *S*-HCQ	77.5	healthy volunteer	single	24	20–36	168 h	0	2
Oral *S*-HCQ	77.5	healthy volunteer	single	72	19–50	77 days	0	3
IV *S*-HCQ	77.5	patient with rheumatoid arthritis	single	32	50±16	32 h	77.7	1

McLachlan et al., 1994[1]; Ducharme et al., 1995[2]; Midha et al., 1996[3]

The qualification of the model was based on comparisons of the observed and predicted pharmacokinetic parameters, shown in Table II, considering the area under the blood concentration-time curve (AUC0–t), and the maximum concentration in blood/plasma (C_{max}). The study design for each simulation, including the percentage of women, the dose, and the age group, was based on data from each published clinical study. The performance of the simulations was assessed by the mean fold error (MFE) for the PK parameters (AUC, C_{max}, and t_{max}) using Equation 3. The PBPK model was considered to perform adequately when all the predicted parameters were within two-fold the corresponding observed value (MFE 0.5–2.0). Another criterion used to evaluate the model was calculating the average error (AFE), which corresponds to an indicator of prediction bias (Equation 4). In general, predictions are considered satisfactory when AFE is between 0.8–1.25. Predictions are considered acceptable with AFE between 0.5–0.8 or 1.25–2.0, and poor when AFE is < 0.5 or > 2. The AAFE (absolute average fold error) calculation (Equation 5), converts the negative values of the log-transformed errors, assessing the dispersion of the predictions. Predictions are satisfactory when AAFE is less than 1.25, acceptable when AAFE is between 1.25 and 2, and poor when AAFE is above 2.

$$Cl_{NR} = Cl_H = Cl_T - Cl_R \qquad \textit{Eq. 3}$$

$$AFE = 10^{\frac{1}{n}\Sigma \log \frac{Pred_i}{Obs_i}} \qquad \textit{Eq. 4}$$

$$AAFE = 10^{\frac{1}{n}\Sigma \left|\log \frac{Pred_i}{Obs_i}\right|} \qquad \textit{Eq. 5}$$

TABLE II - Model verification for HCQ enantiomers. The table shows the predicted and observed data and the mean fold error (MFE) in relation to the kinetic characteristics discussed

Administration route/compound	Matrix	Dose (mg)	Ref.	AUC Predicted (ng. h/mL)	AUC observed (ng. h/mL)	Cmax predicted (ng/mL)	Cmax observed (ng/mL)	MFE AUC	MFE Cmax
R-HCQ oral	Blood, 0–168 h	77.5	1	3976.18	3948	90.23	84	**1.01**	**1.22**
R-HCQ oral	Blood, 0–168 h	77.5	2	4028.91	4245.16	90.88	164.55	**0.94**	**0.55**
R-HCQ IV	Blood, 0–32 h	77.5	3	2636.09	3444.49	-	-	**0.76**	**-**
AFE								**0.90**	**0.81**
AAFE								**1.11**	**1.22**

Administration route/compound	Matrix	Dose (mg)	Ref.	AUC Predicted (ng. h/mL)	AUC observed (ng. h/mL)	Cmax predicted (ng/mL)	Cmax observed (ng/mL)	MFE AUC	MFE Cmax
S-HCQ oral	Blood 0–168 h	77.5	1	1966.36	2208	79.81	52	**0.89**	**1.5**
S-HCQ oral	Blood 0–168 h	77.5	2	2000.89	2813.74	80.48	105.96	**0.71**	**0.75**
S-HCQ IV	Blood 0–32 h	77.5	3	1959.79	1875.2	-	-	**1**	**-**
AFE								**0.85**	**1.06**
AAFE								**1.16**	**1.06**

AUC: area under the curve. Cmax: maximum concentration. AFE: average-fold error. AAFE: absolute average-fold error.

Simulations

The simulation was conducted to assess the kinetic disposition of *R*- and *S*–HCQ in different CYP2D6 phenotypes. Each phenotype, including poor metabolizers (PMs), normal metabolizers (NMs), or ultrafast metabolizers (UMs), was assigned a frequency in the population of 1 or 100%. The assignment of these frequencies was in accordance with the CYP2D6 frequency table (PharmGKB database). Similarly, the kinetics of *R*- and *S*-HCQ in different CYP2C8 phenotypes were investigated (Rodriguez-Antona *et al...,* 2008). Frequencies of 1 were assigned to each phenotype (NM and PM). The simulation encompassed 1000 subjects, divided into ten trials, each comprising 100 volunteers aged between 20 and 50 years old. The participant pool was composed of 50% women. The simulation was carried out for a single dose of 200 mg HCQ sulfate (corresponding to 77.5 mg *R*- and 77.5 mg *S*–HCQ) and generated blood concentration versus time profiles over 216 hours post-administration.

A simulation was conducted to investigate the impact of the CYP3A4 inhibitor drug clarithromycin (CLTR) on the kinetic disposition of *R*- and *S*–HCQ, with the CLTR data available in the software library. The simulation encompassed 100 subjects, divided into ten trials with ten volunteers each, and the study extended over 216 hours. A single dose of 250 mg of CLTR was administered with 200 mg HCQ sulfate (corresponding to 77.5 mg *R*- and 77.5 mg *S*–HCQ). Relevant drug-specific data for CLTR were readily available within the simulator library. A strong, moderate and weak inhibition effects were defined as per the FDA guidance for clinical drug interaction studies (CDER, 2020).

RESULTS

The blood concentration-time profiles of *R*- and *S*–HCQ after intravenous and oral racemic HCQ administration are depicted in Figure 2. Overall, the models describe well the pharmacokinetics of both *R*- and *S*–HCQ after intravenous administration (Figure S3, Supplementary material). After oral administration, there is a high variability between the observed data from existing literature, especially for *R*-HCQ. Thus, while the model captures the observed data for one study (Ducharme *et al...,* 1995), it is underpredicting the exposure to *R*-HCQ in the other (Midha *et al...,* 1996, Figure 2). Model simulations yielded MFE values within the defined range of 0.5 to 2.0fold, indicating the robustness of the models developed (Figure S3, Supplementary material). Moreover, the AFE values are within 0.8–1.25, showing

that the model accurately estimated the PK parameters AUC and C_{max}. The AAFE values within the range of 1–1.25 also suggested that the simulations satisfactorily describe the observed data (Table II).

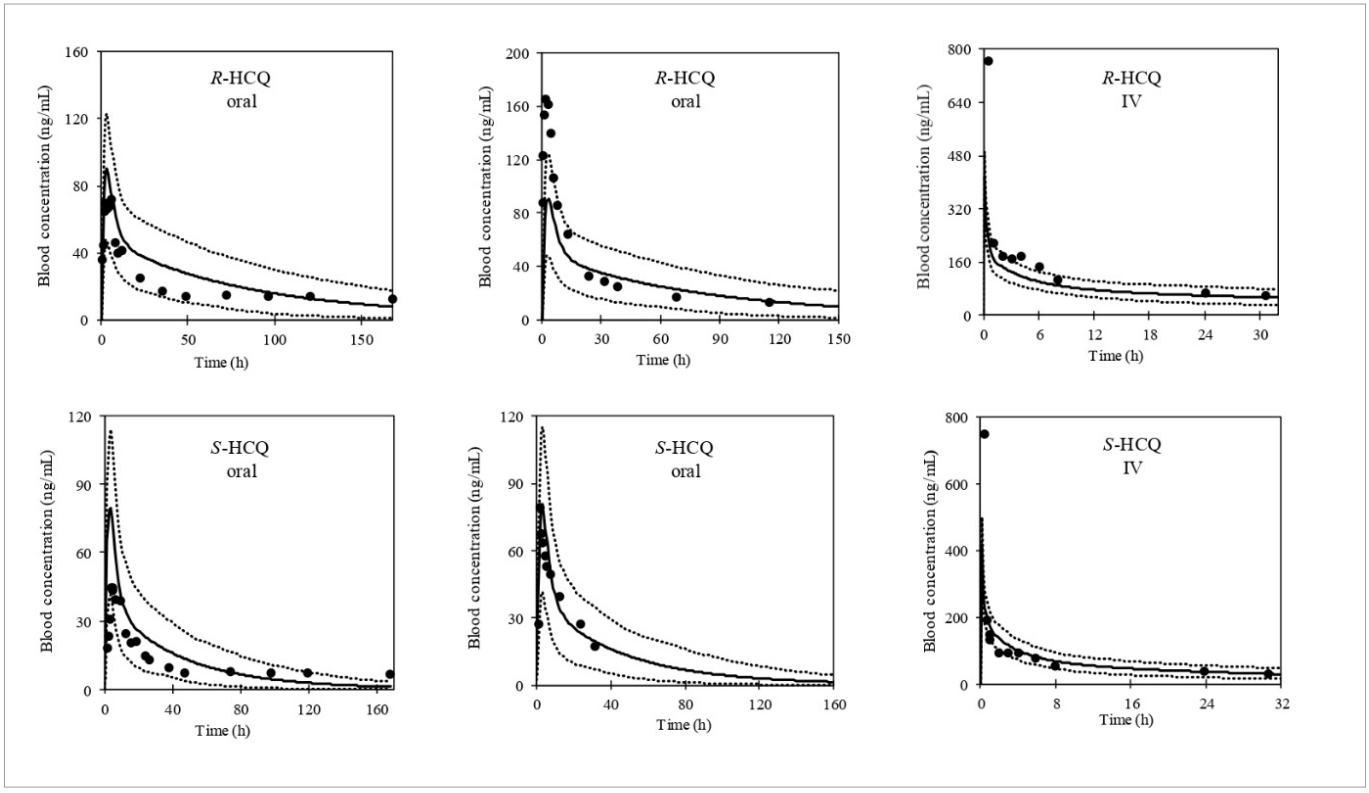

FIGURE 2 - Predicted and observed blood concentration data of *R*–HCQ and *S*–HCQ after oral and IV administration. The straight line represents the predicted median concentration, and the dashed lines represent the 5th and 95th percentiles. Observed data are represented as black circles. (1) Ducharme *et al...*, 1995; (2) Midha *et al...*, 1996; (3) McLachlan *et al...*, 1994.

The prediction of Fa yielded values of 0.77 for both *R*–HCQ and *S*–HCQ using the first-order absorption model. This model effectively captured the oral absorption of *R*-HCQ and *S*-HCQ, as no enantioselectivity has been described in this process. Observed Fa values were closely aligned with the simulated Fa values, 0.74 and 0.77 for *R*–HCQ and *S*–HCQ, respectively (McLachlan *et al...*, 1994). The C_{max} values of *R*–HCQ and *S*–HCQ were sensitive to the incorporation of subcellular distribution into lysosomes due to an increase in the volume of distribution (Supplementary material, Figure S1).

Subcellular distribution with HCQ trapping in the liver, kidney, and lung was incorporated in the distribution method 3 with ionic permeability. By adding the subcellular distribution, there was a substantial increase in the tissue:plasma partition coefficient in tissues with high lysosomal content, significantly altering the local exposure to the drug. Our simulations suggest that distribution, not clearance, is the primary determinant of enantioselectivity for HCQ. Although a significant difference in blood exposure is observed between *R*- and *S*-HCQ, plasma exposure is similar between the enantiomers (Supplementary material, Figure S2).

The final PBPK model for both *R*-HCQ and *S*-HCQ was utilized to investigate the influence of genetic polymorphisms in CYP2D6 and CYP2C8. Notably, individuals with CYP2D6 PM status exhibited a 1.3-fold increase in the AUC for both *R*-HCQ and *S*-HCQ

compared to those with NM status. Conversely, individuals with UM status of CYP2D6 showed a 0.9-fold reduction in the AUC for both enantiomers of HCQ. In the case of CYP2C8, PBPK simulations for the PM phenotype revealed a weak inhibition with 1.5-fold increase in the AUC for *R*-HCQ and a 1.6-fold increase for *S*-HCQ compared to individuals with the NM phenotype (Figure 3; Supplementary material, Table SIII). Further simulations were conducted for a scenario where both CYP2C8 and CYP2D6 were in the PM state (Figure 4). In this context, a 2-fold increase in AUC was observed for the *R*-HCQ enantiomer and a 2.3-fold increase for the *S*-HCQ enantiomer, relative to individuals with NM phenotypes for both CYP2C8 and CYP2D6, indicating a moderate drug-gene interaction within this subgroup.

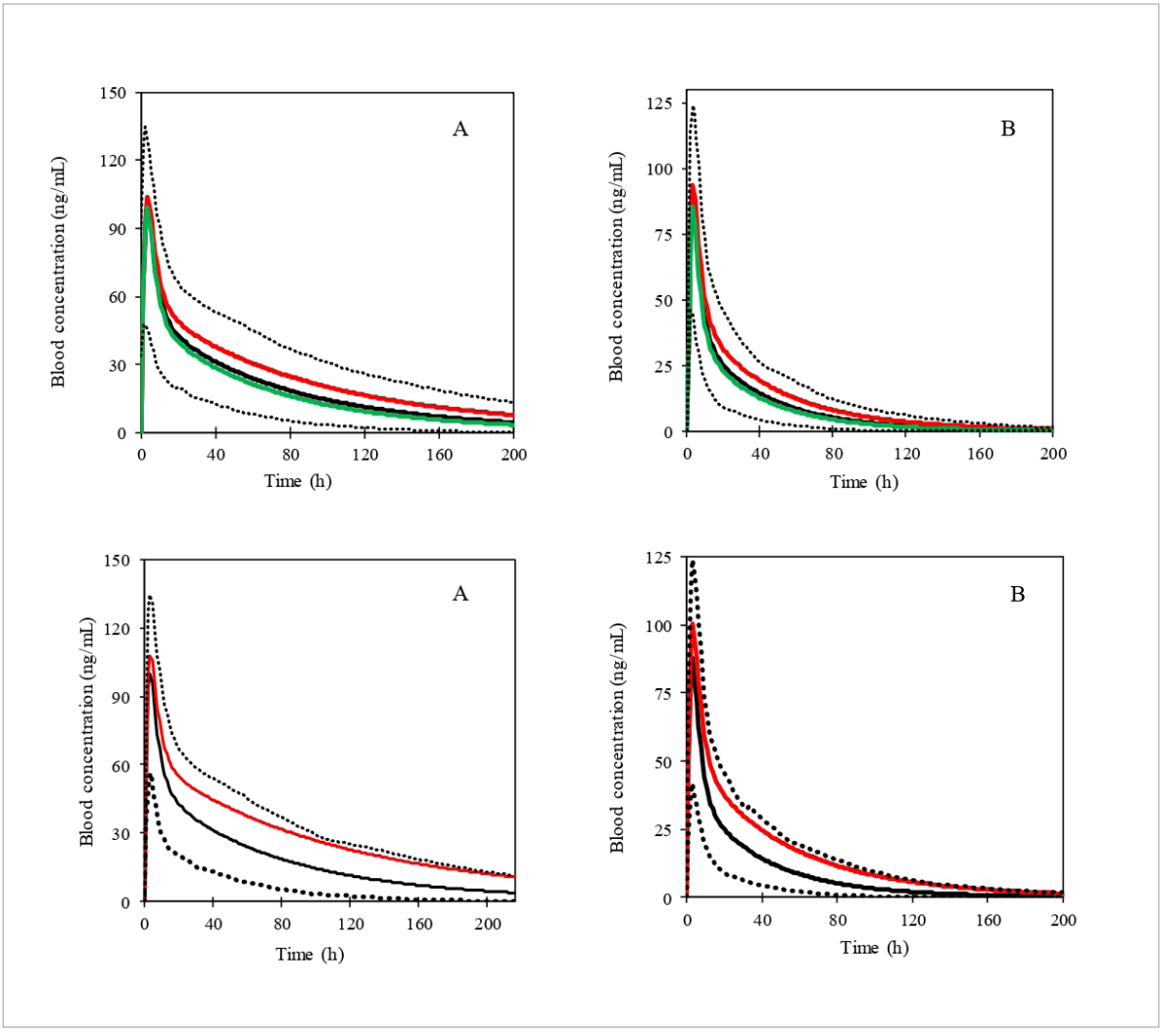

FIGURE 3 - Effect of CYP2D6 and CYP2C8 metabolizing phenotypes on exposure to *R*–HCQ and *S*–HCQ. The upper plots depict the simulation of CYP2D6 activity on the kinetic disposition of *R*–HCQ (A) and *S*–HCQ (B) in blood after oral administration. The bottom graphs show the simulation of the effect of CYP2C8 activity on the kinetic disposition of *R*–HCQ (A) and *S*–HCQ (B) in blood after oral administration. Ultrafast metabolizers (UM) are shown in green; normal metabolizers (NM) in black; and poor metabolizers (PM) in red. The dashed lines represent the 5th and 95th percentile values relative to the NM.

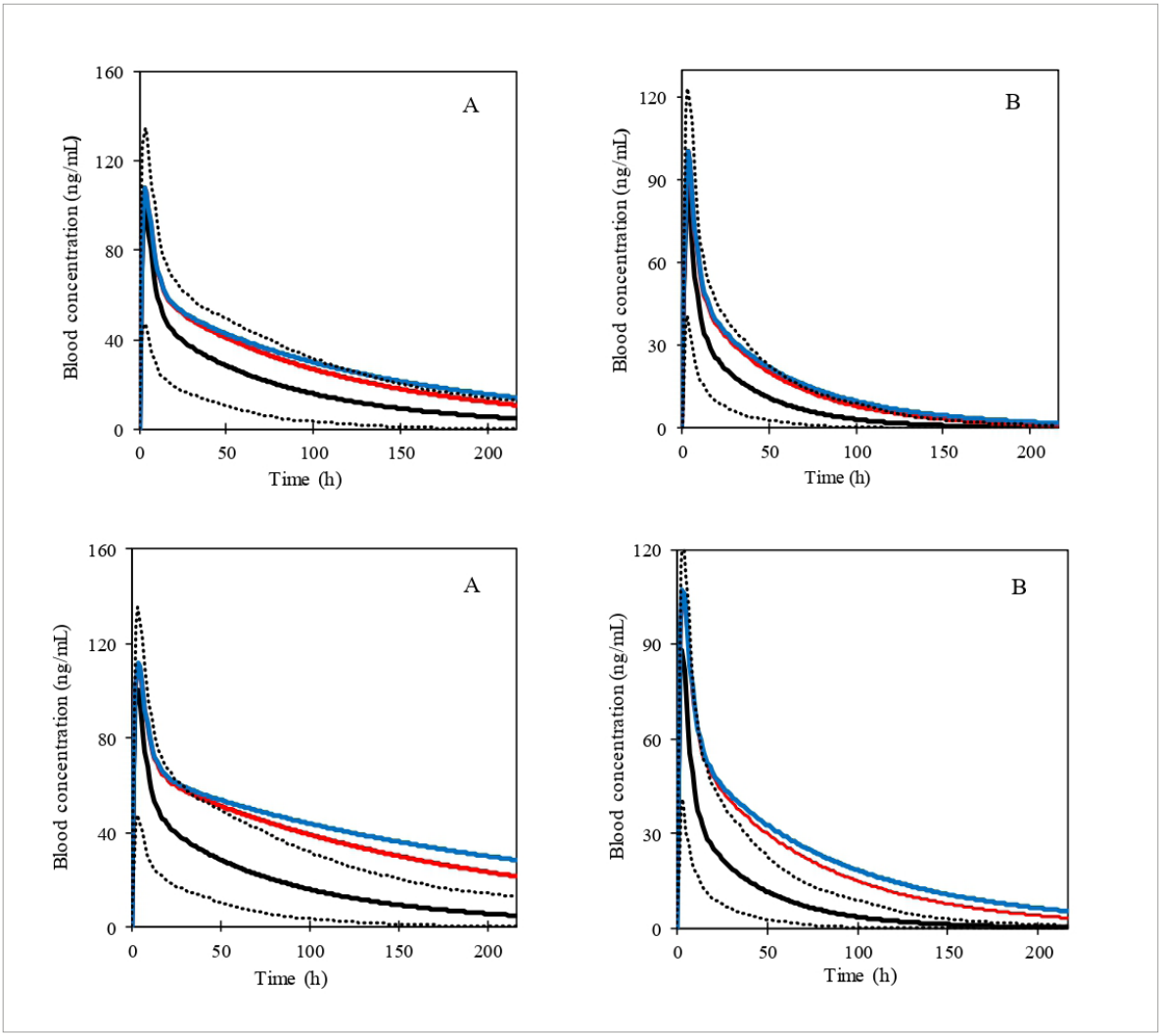

FIGURE 4 - Effect of CYP2D6 and CYP2C8 gene expression in the presence of a CYP3A4 inhibitor. The upper graphs show blood concentration-time profiles of *R*-HCQ (A) and *S*-HCQ (B) in CYP2C8 PM in the absence (red) and in the presence (blue) of a CYP3A4 inhibitor. Normal metabolizers for CYP2C8 are represented in the black solid line with the respective predicted 5th and 95th percentiles (dashed lines). The lower graphs show the blood concentration-time profiles of *R*-HCQ (A) and *S*-HCQ (B) of CYP2C8 PM/CYP2D6 PM in the absence (red) in the presence (blue) of a CYP3A4 inhibitor. The black solid lines represent normal metabolizers for CYP2C8 and CYP2D6. The dashed lines represent the 5th and 95th percentiles for CYP2C8 NM/CYP2D6 NM.

To explore the worst-case scenarios, we examined populations with the PM phenotype for CYP2C8 in the presence of CLTR, a CYP3A4 inhibitor, resulting in a weak inhibition with 1.7-fold increase in AUC for both HCQ enantiomers compared to those with CYP2C8 NM phenotypes. Furthermore, we assessed the coadministration of CLTR and HCQ in the PM state for both CYP2C8 and CYP2D6. Under these conditions, where the metabolism of all major pathways for *R*-HCQ and *S*-HCQ was impaired, the AUC for *R*-HCQ increased by 2.34-fold, and for *S*-HCQ, it increased by 2.68-fold, relative to individuals with NM phenotypes indicating a moderate inhibition (Figure 5, Supplementary material, Table SIII).

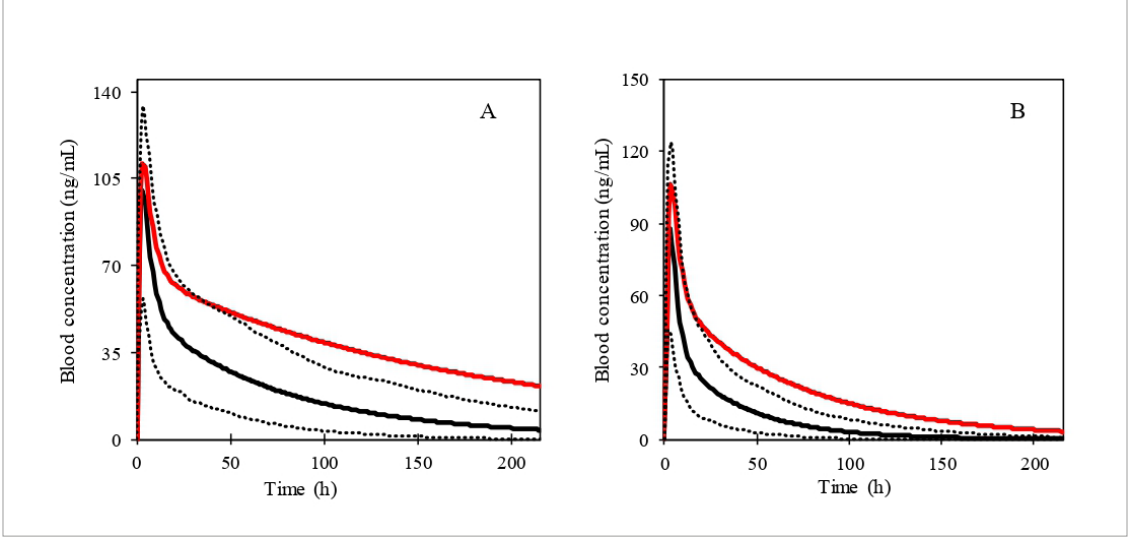

FIGURE 5 - Blood concentration-time profiles in poor metabolizers (PM) for both CYP2C8 and CYP2D6 after oral administration for *R*–HCQ (A) and *S*–HCQ (B). The black line represents the median values for NM for CYP2C8 and CYP2D6; the red line represents a PM CYP2C8 and PM CYP2D6; dashed lines depict the 5th and 95th percentile values relative to the NM for CYP2C8 and CYP2D6**.**

DISCUSSION

PBPK models were developed to predict the concentration-time profiles and PK parameters of *R*–HCQ and *S*–HCQ in humans. The model development was based on clinical data and in vitro assays that investigated enantioselectivity on the kinetic disposition of HCQ. Due to the lack of in vitro metabolism data for the individual enantiomers of HCQ, a backward extrapolation strategy was employed to incorporate enzymatic kinetic data. This strategy was based on the observation that the hepatic clearance of HCQ in plasma is not enantioselective. As expected, the molecular weight, log P, and pKa values are identical for racemic HCQ, R-HCQ, and S-HCQ. HCQ is a highly lipophilic drug with an octanol:water partition coefficient (log P) of 3.84. According to the Biopharmaceutics Classification System (BCS), it is a class 1 drug, meaning it has high solubility and high permeability. The Fa of 0.74 for R-HCQ and 0.77 for S-HCQ in patients with rheumatoid arthritis (McLachlan *et al...,* 1994) was well captured in the current model.

The enantioselective distribution pattern is attributed to the discrepancies in unbound fraction in plasma and blood:plasma concentration ratio between HCQ enantiomers. *S*–HCQ displays a higher affinity to plasma proteins (Li *et al...*, 2015**)**. Following both oral and intravenous administration of *racemic*-HCQ, blood concentrations of *R*–HCQ are higher compared to *S*–HCQ, which can be explained by the enantioselective distribution of HCQ to blood cells and other tissues (Ducharme *et al...*, 1995; McLachlan *et al...*, 1994; Midha *et al...*, 1996). By employing method 3 as a distribution model, the predicted values of Vd were 97.9 L/kg and 54.1 L/kg for *R*-HCQ and *S*-HCQ, respectively. These values align with observations in blood for the enantiomeric mixture in both COVID-19 patients and healthy volunteers (Munster *et al...*, 2002; Zahr *et al...*, 2021**)**. The pronounced distribution of HCQ can be explained by lysosomal sequestration, a phenomenon previously described for aminoquinolines (MacIntyre, Cutler, 1988). Because it is a diprotic base at physiological pH, HCQ can accumulate in lysosomes at concentrations up to 50,000-fold higher than cytosolic and extracellular concentrations (Derendorf, 2020**)**.

Lysosomes are abundant in the liver, lungs, kidneys, and spleen. Drug sequestration in lysosomes occurs mainly for weak bases that ionize preferentially at the acidic lysosomal pH. Because of the low permeability of ionized compounds, these compounds are trapped in the lysosome, contributing to the increased distribution of these drugs, especially to tissues with high lysosomal content (MacIntyre, Cutler, 1988). It must be considered that the site of action of aminoquinolines depends on the therapeutic indication. In the pharmacological treatment of arthritis, monocytes and lymphocytes are believed to represent target tissues for HCQ. In vitro cell distribution data suggest that HCQ has superior cellular uptake for these cells in the blood compared to erythrocytes (Brocks, Mehvar, 2003).

The absence of enzyme kinetics data for the HCQ enantiomers is a limitation in the current models. However, as the hepatic clearance in plasma remains comparable for both enantiomers, metabolism is unlikely to account for the enantioselective pharmacokinetics. Simulation outcomes with the PBPK model reveal a substantial disparity in blood exposure between *R*- and *S*–HCQ, yet plasma exposure remains similar for both enantiomers (Figure 2). Considering that the hepatic blood flow typically ranges from 60 to 90 L/h, while the hepatic clearance in blood was 12.76 L/h and 22.6 L/h for *R*–HCQ and *S*–HCQ, respectively (McLachlan *et al.*..., 1993), it becomes evident that *R*–HCQ and *S*–HCQ are low hepatic extraction ratio (ER) drugs. Given this profile, where the hepatic clearance hinges predominantly on intrinsic clearance and the fraction unbound, we can deduce that the extensive distribution of the drug to the blood cells constrains the hepatic clearance of HCQ.

Nevertheless, these observations contrast the findings of Cardoso and Bonato (2009), who proposed in vitro enantioselective metabolism with a preference for metabolizing *R*–HCQ (Cardoso, Bonato, 2009). However, it is essential to recognize that these authors did not ascertain the fraction of free drug within the microsomal medium, an element that could substantially influence experimental outcomes. Moreover, the authors did not determine the essential enzymatic kinetics parameters Km and Vmax, hampering a comprehensive characterization of the metabolism of both *R*–HCQ and *S*–HCQ.

Simulations with CYP2D6 PM subjects showed an increase in the AUC of *R*–HCQ and *S*–HCQ compared to CYP2D6 NMs (Figure 3). CYP2D6 UM individuals showed a reduction in the AUC of *R*–HCQ and *S*–HCQ. This result may corroborate an analysis conducted on 194 Korean patients with lupus erythematosus treated with HCQ, revealing an association between the [DHCQ]:[HCQ] ratio and the CYP2D610 polymorphism (rs1065852) (Lee *et al.*..., 2015). Specifically, individuals carrying the G/G genotype of this polymorphism (wild-type allele) showed elevated [DHCQ]:[HCQ] ratios compared to the A/A or A/G genotypes (Lee *et al...,* 2015). It is important to note that the prevalence of the CYP2D610 variant allele is significantly high among Asian populations, reaching 78% (Llerena *et al.*..., 2014). This high prevalence contributes to increased HCQ exposure in Asian individuals due to reduced CYP2D6 expression among carriers of the CYP2D6*10 allele. In a modeling and simulation study, quinidine, a potent CYP2D6 inhibitor, and ritonavir, a weak CYP2D6 inhibitor, were used as investigative agents. When co-administered with HCQ, the results indicated a marginal 19% increase in systemic HCQ exposure in healthy volunteers. Thus, the effect found in this simulation study for the pharmacogenetics-related reduction of CYP2D6 activity resembles the effect of CYP2D6 inhibition in a PBPK model for the enantiomeric mixture (Zhang *et al...,* 2021).

PBPK simulations for the PM CYP2C8 phenotype also showed a slight increase in the AUC of R- and S-HCQ compared to individuals with the NM CYP2C8 phenotype (Figure 3), which can be compared to a study where specific *2, *3, *4, and *8 CYP2C8 alleles showed reduced metabolic activity for some CYP2C8-dependent substrates in vitro (Rodriguez-Antona *et al.*..., 2008; Tornio *et al...,* 2008). Notably, the *2 allele is more prevalent in African Americans, while the *3 allele exhibits a higher frequency among Caucasians (Rodriguez-Antona *et al...,* 2008). Despite these findings, due to the limited availability of in vivo and in vitro data on CYP2C8 variants and their functional implications, these alleles

are not definitively linked to distinct phenotypes, such as PM or UM metabolizers (Aquilante *et al...,* 2013). PBPK simulations were conducted with gemfibrozil as a CYP2C8 inhibitor in different scenarios of drug-drug interactions with HCQ (Zhang *et al...,* 2021). When gemfibrozil (600 mg twice daily) is administered simultaneously with HCQ (at an initial dose of 600 mg twice daily, followed by maintenance doses of 200 mg twice daily for four days), there was approximately a 20% increase in the AUC of HCQ compared to sole HCQ administration in healthy adults. Of particular interest, the interaction between gemfibrozil and HCQ exhibited a more pronounced effect among elderly subjects aged between 85 and 95 years. In this age group, the concurrent use of gemfibrozil and HCQ resulted in an average AUC increase of 56% compared to subjects exclusively receiving HCQ (Zhang *et al...,* 2021).

Exposure and toxicity data are scarce for HCQ. Acute poisoning cases have been documented, with reported plasma concentrations of 9.87×10^3 µg/mL at 2 hours, 4.53×10^3 µg/mL at 10 hours, and 6.4×10^2 µg/mL at 68 hours after a patient ingested approximately 1, 200 mg of HCQ (Jordan *et al...*, 1999). Severe toxicity has been reported in patients exhibiting plasma levels from 6.4×10^2 to 6.1×10^3 µg/mL, while fatal cases have demonstrated post-mortem blood levels of 4.8×10^4 µg/mL and 10^5 µg/mL (Miller, Fiechtner, 1989; Kemmenoe, 1990). One study showed that patients with rheumatoid arthritis (RA) who had been on HCQ therapy for six months with weekly doses of 3,000 mg of *racemic*HCQ had *R*–HCQ and *S*–HCQ concentrations of approximately 1,000 ng/mL and 800 ng/mL, respectively (Tett *et al...*, 1994). However, there is no precise information in the literature regarding the toxicity of HCQ enantiomers (McLachlan *et al...*, 1993). Another study conducted with patients with RA found that doses of 200 mg daily were sufficient for significant pain reduction at rest and in motion and that daily doses of 400 mg did not result in improved therapy (Tett *et al...*, 2000). The available studies show that the PKPD relationship for the different therapeutic indications of HCQ is not yet well defined. Pharmacodynamic data specific to each enantiomer is lacking. It is also unclear whether systemic exposure can be predictive of HCQ toxicity. Consequently, the model's implications for dose adjustment and optimization necessitate further research that explores the pharmacokinetic targets associated with efficacy and safety considerations.

Our model-based approach provided a unique opportunity to explore complex scenarios that might be challenging to evaluate through clinical studies alone. These intricate scenarios included instances where genetic polymorphisms were concurrently present in the CYP2D6 and CYP2C8 genes. Additionally, the simulation delved into the complex effects of CYP3A4 inhibition on distinct phenotypes within the CYP2C8 and CYP2D6 pathways. This approach facilitated examining interactions that might not be easily studied under traditional clinical conditions. The current study has some limitations. The PBPK models developed hinged upon the assumption of equal enzymatic contributions from CYP2D6, CYP2C8, and CYP3A4 for both enantiomers, driven by the observed non-enantioselective plasma clearance. Nevertheless, for the future refinement of the model, there is a clear need for in-depth in vitro metabolism studies to unravel the distinct enzymatic kinetics governing *R*- and *S*–HCQ. The lack of currently available data restricts model verification to the scope of a few clinical investigations. Consequently, applying the model's outcomes for dose adjustment remains constrained. This limitation arises from the fact that both pharmacological and safety-related molecular targets are inadequately characterized. Moving forward, a more comprehensive understanding of these critical aspects is essential to maximize the model's significance in informing dosage adjustments and optimizing HCQ therapy.

ACKNOWLEDGMENTS

This study was financed in part by the Coordenação de Aperfeiçoamento de Pessoal de Nível Superior - Brasil (CAPES) - Finance Code 001.

Author contributions

GSGR: conceptualization, formal analysis, interpretation of data, original draft, and writing review & editing
LFP: interpretation of data, and critical article revision
FLM interpretation of data, and critical article revision
NVM: conceptualization, data analysis, interpretation of data, and critical article revision

REFERENCES

Aquilante CL, Niemi M, Gong L, Altman RB, Klein TE. PharmGKB summary. Pharmacogenet Genomics. 2013;23(12):721-728.

Brocks DR, Mehvar R. Stereoselectivity in the pharmacodynamics and pharmacokinetics of the chiral antimalarial drugs. Clin Pharmacokinet. 2003;42:1359-1382.

Brocks DR, Skeith KJ, Johnston C, Emamibafrani J, Davis P, Russell AS, et al. Hematologic disposition of hydroxychloroquine enantiomers. J Clin Pharmacol. 1994;34(11):1088-1097.

Cardoso CD, Bonato PS. Enantioselective metabolism of hydroxychloroquine employing rats and mice hepatic microsomes. Rev Bras Cienc Farm. 2009;45:658-667.

CDER. Clinical Drug Interaction Studies — Cytochrome P450 Enzyme- and Transporter-Mediated Drug Interactions Guidance for Industry. U.S. Department of Health and Human Services, Food and Drug Administration, Center for Drug Evaluation and Research. January 2020.

Derendorf H. Excessive lysosomal ion-trapping of hydroxychloroquine and azithromycin. Int J Antimicrob Agents. 2020;55(6):106007.

Ducharme J, Fieger H, Ducharme MP, Khalil SK, Wainer IW. Enantioselective disposition of hydroxychloroquine after a single oral dose of the racemate to healthy subjects. Br J Clin Pharmacol. 1995;40:127-133.

Hughes E, Wallender E, Mohamed A, Jagannathan P, Savic RM (2021). Malaria PK/PD and the role pharmacometrics can play in the global health arena: malaria treatment regimens for vulnerable populations. Clin Pharmacol Ther. 2021;110(4):926-940.

Jordan P, Brookes JG, Nikolic G, Le Couteur DG. Hydroxychloroquine overdose: toxicokinetics and management. J Toxicol Clin Toxicol. 1999;37(7):861-864.

Kemmenoe AV. An infant fatality due to hydroxychloroquine poisoning. J Anal Toxicol. 1990;14(3):186-188.

Lee JY, Vinayagamoorthy N, Han K, Kwok SK, Ju JH, Park KS, et al. Association of Polymorphisms of Cytochrome P450 2D6 With Blood Hydroxychloroquine Levels in Patients With Systemic Lupus Erythematosus. Arthritis Rheumatol. 2015;68(1):184-190.

LLerena A, Naranjo ME, Rodrigues-Soares F, Penas-LLedó EM, Fariñas H, Tarazona-Santos E. Interethnic variability of CYP2D6 alleles and of predicted and measured metabolic phenotypes across world populations. Expert Opin Drug Metab Toxicol. 2014;10(11):1569-1583.

Li DQ, Kim R, McArthur E, Fleet JL, Bailey DG, Juurlink D, et al. Risk of adverse events among older adults after co-prescription of clarithromycin and statins not metabolized by cytochrome P450 3A4. Cmaj. 2015;187(3):174-180.

MacIntyre AC, Cutler DJ. The potential role of lysosomes in tissue distribution of weak bases. Biopharm Drug Dispos. 1988;9(6):513-526.

McLachlan AJ, Cutler DJ, Tett SE. Plasma protein binding of the enantiomers of hydroxychloroquine and metabolites. Eur J Clin Pharmacol. 1993;44(5):481-484.

McLachlan AJ, Tett SE, Cutler DJ, Day. Disposition and absorption of hydroxychloroquine enantiomers following a single dose of the racemate. Chirality. 1994;6:360-364.

Madabushi R, Seo P, Zhao L, Tegenge M, Zhu H.. Role of model-informed drug development approaches in the lifecycle of drug development and regulatory decision-making. Pharm Res. 2022;39(8):1669-1680.

Midha KK, Hubbard JW, Rawson MJ, McKay G, Schwede R.. The roles of stereochemistry and partial areas in a parallel design study to assess the bioequivalence of two formulations of hydroxychloroquine: a drug with a very long half-life. Eur J Pharm Sci. 1996;4(5):283-292.

Miller D, Fiechtner J. Hydroxychloroquine overdosage. J Rheumatol. 1989;16(1):142-143.

Munster T, Gibbs JP, Shen D, Baethge BA, Botstein GR, Caldwell J, et al. Hydroxychloroquine concentration–response relationships in patients with rheumatoid arthritis. Arthritis Rheum. 2002;46(6):1460-1469.

Rodriguez-Antona C, Niemi M, Backman JT, Kajosaari LI, Neuvonen PJ, Robledo M, et al. Characterization of novel CYP2C8 haplotypes and their contribution to paclitaxel and repaglinide metabolism. The pharmacogenomics journal. 2008; 8(4): 268-277.

Ruiz-Irastorza G, Ramos-Casals M, Brito-Zeron P, Khamashta MA. Clinical efficacy and side effects of antimalarials in systemic lupus erythematosus: a systematic review. Ann Rheum Dis. 2010;69(1):20-28.

Tanaka E, Taniguchi A, Urano W, Yamanaka H, Kamatani N. Pharmacogenetics of disease-modifying anti-rheumatic drugs. Best Pract Res Clin R. 2004;18(2):233-247.

Tett SE, Cutler DJ, Beck C, Day RO. Concentration-effect relationship of hydroxychloroquine in patients with rheumatoid arthritis: a prospective, dose-ranging study. J Rheumatol. 2000;27(7):1656-1660.

Tett SE, McLachlan AJ, Cutler DJ, Day ROT. Pharmacokinetics and pharmacodynamics of hydroxychloroquine enantiomers in patients with rheumatoid arthritis receiving multiple doses of racemate. Chirality. 1994;(6):355-359.

Tornio A, Niemi M, Neuvonen PJ, Backman JT. Trimethoprim and the CYP2C8* 3 allele have opposite effects on the pharmacokinetics of pioglitazone. Drug Metabolism and Disposition. 2008;36(1):73-80.

Toutain PL, Bousquet-Mélou A. Plasma clearance. J Vet Pharmacol Ther. 2004;27(6):415-425.

Zahr N, Urien S, Llopis B, Pourcher V, Paccoud O, Bleibtreu A, et al. Pharmacokinetics and pharmacodynamics of hydroxychloroquine in hospitalized patients with COVID-19. Therapies. 2021;76(4):285-295.

Zhang M, Yao X, Hou Z, Guo X, Tu S, Lei Z, et al. Development of a physiologically based pharmacokinetic model for hydroxychloroquine and its application in dose optimization in specific COVID-19 patients. Front Pharmacol. 2021;11:585021.

Received for publication on 13th May 2024
Accepted for publication on 17th July 2024
Associated Editor: Silvya Stuchi Maria-Engler

Supplementary material

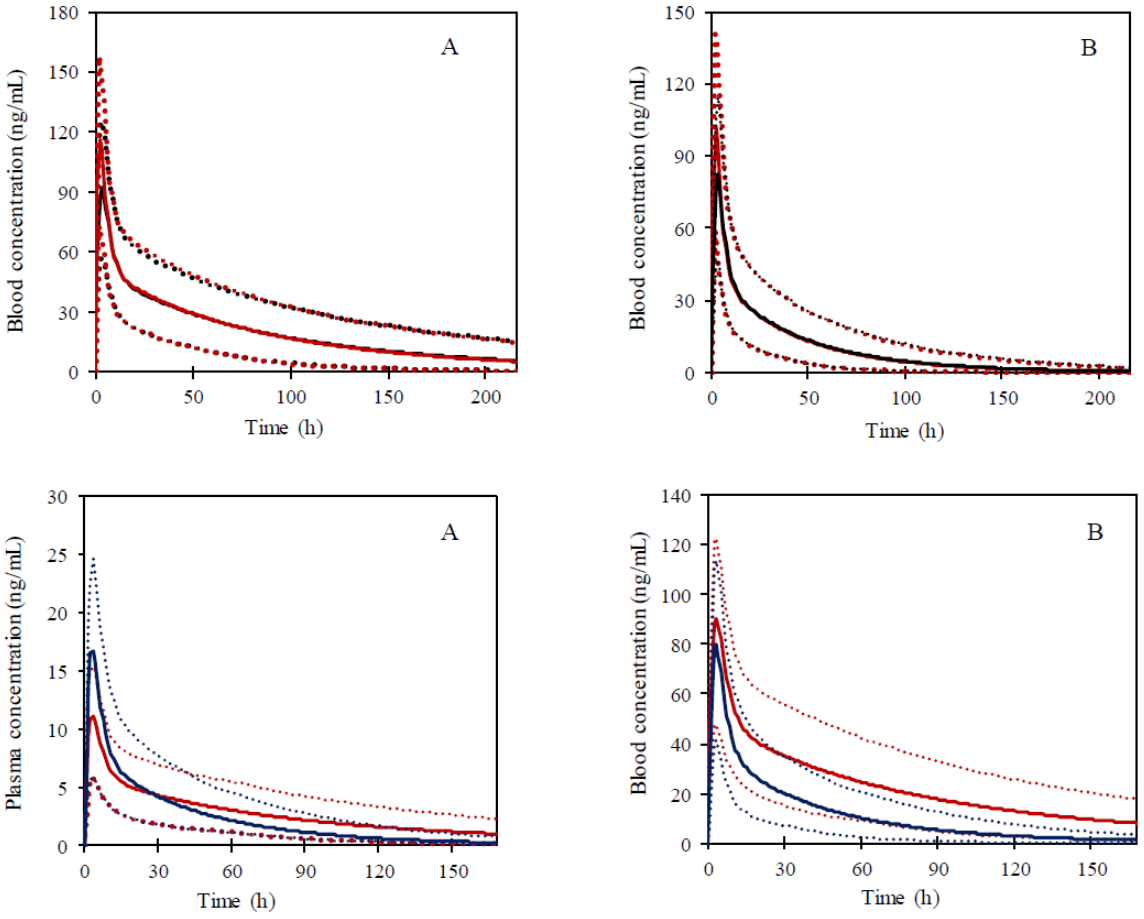

FIGURE S1 - Blood concentration-time profiles for *R*-HCQ (A) and *S*-HCQ (B) after oral administration of HCQ. The red line represents the simulation before incorporating subcellular distribution into the model and the black line after adding subcellular distribution. The dashed lines represent the 5th and 95th percentiles.

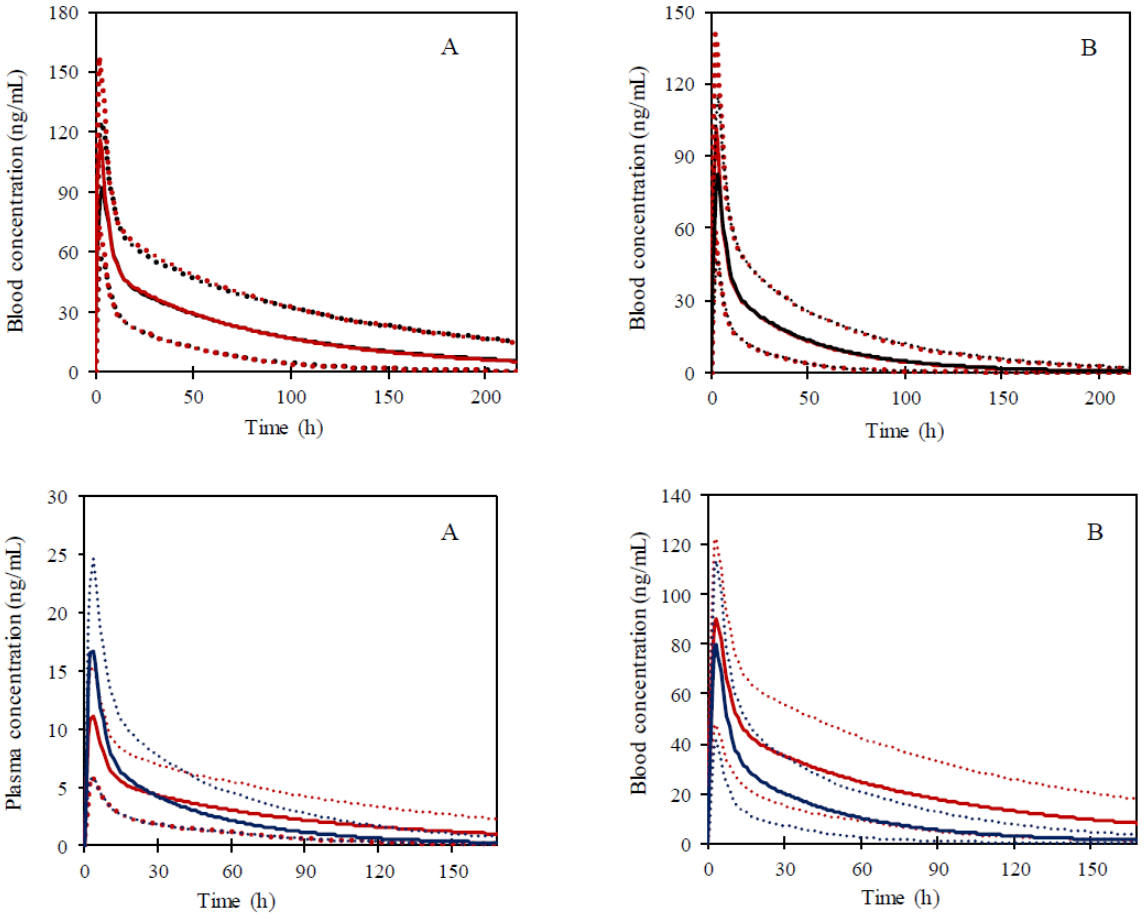

FIGURE S2 - Concentration profiles of *R*-HCQ (red) and *S*-HCQ (dark blue) in plasma (A) and in blood (B). The dotted lines represent the 5th and 95th percentiles.

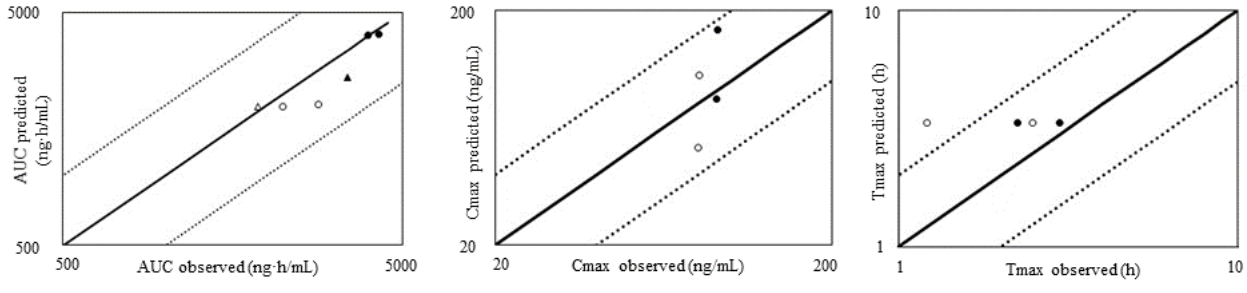

FIGURE S3 - PBPK model verification of *R*–HCQ and *S*–HCQ enantiomers. The simulated and observed PK parameters were used to verify the final PBPK model. Solid lines represent the unit line, dashed lines represent the 0.5fold and 2fold difference. *R*–HCQ is represented by filled symbols, and *S*–HCQ by empty symbols. Oral administration data are represented by circles, and intravenous administration data by triangles.

TABLE SI - Parameters used to construct HCQ enantiomers

Parameters	*R*-HCQ	*S*-HCQ	Reference
Physico-chemical properties			
Molecular weight (g/mol)	335.87	335.87	PubChem Compound
Log P	3.84	3.84	PubChem Compound
Compound type	Diprotic base	Diprotic base	PubChem Compound
pKa	9.67 (pKa 1) 8.27 (pKa 2)	9.67 (pKa 1) 8.27 (pKa 2)	PubChem Compound
Blood binding properties			
Blood to plasma ratio (B/P)	8.6	5	Tett *et al...,* 1998. Estimated data for the enantiomers
Unbound fraction in plasma	0.63	0.36	McLachlan *et al...,* 1993
Absorption			
Model	First-order	First-order	
Fraction absorbed (Fa)	0.74 (30%)	0.77 (30%)	McLachlan *et al...,* 1994
Ka (1/h)	0.3 (30%)	0.3 (30%)	Adjusted for in vivo data
Lag time (h)	0.5 (30%)	0.5 (30%)	
Distribution			
Model	Whole-body	Whole-body	
Vss (L/kg)	97.89	54.07	Predicted value
Subcellular distribution	Activated	Activated	Rodgers *et al...*, 2005
Kp scalar	0.44	0.44	
Prediction method	Method 3	Method 3	Rodgers *et al...,* 2005
Elimination			
Clearance	Enzyme kinetics	Enzyme kinetics	
$Cl_{total,plasma}$ (L/h)	130.45	175.7	Midha *et al...*, 1996
$CL_{int,CYP2C8}$ (µL/min/pmol)	0.927	1.96	Retrograde extrapolation
% contribution CYP2C8	46.4	44.2	
$CL_{int,CYP2D6}$ (µL/min/pmol	1.091	2.308	Retrograde extrapolation
% contribution CYP2D6	24.0	22.9	
$CL_{int,CYP3A4}$ (µL/min/pmol)	0.061	0.129	Retrograde extrapolation
% contribution CYP3A4	20.7	19.8	
$Cl_{int,additionalHLM}$ (µL/min/mg protein)	3.232	10.554	Parameter identification to capture data
Typical renal clearance (L/h)	15.4	23.0	Calculation based on plasma data Ducharme *et al...,* 1995

Log P: Partition coefficient. pKa: Acid dissociation constant. Vss: Apparent volume of distribution at steady state. CLint: intrinsic clearance Ka: absorption constant. Lag time: latency time.

TABLE SII - Review of literature data on total, renal and hepatic clearance values of HCQ enantiomers in plasma and blood

	Reference	*R*-HCQ	*% of* Cl_T	*S*-HCQ	*% of* Cl_T	*R/S*	Matrix	Observations
CL_R	McLachlan et al. 1993	1.14 L/h	8.2%	2.46L/h	8.2%	0.46	IV, blood	Observed
CL_T		13.9 L/h	-	25.1 L/h	-	0.55		Observed
CL_H		12.76 L/h	91.8%	22.64 L/h	90.2%	0.56		Calculated
CL_R	McLachlan et al. 1993	9.8 L/h		12.3 L/h		0.79	IV Plasma	Calculated with B/P
CL_T		119.5 L/h	-	127 L/h	-	0.94		Observed
CL_H		109.7 L/h	91.8 %	114.7 L/h	90.3 %	0.95		Calculated
CL_R	Ducharme et al. 1995	1.79 L/h	9.1 %	4.61 L/h	13.13%	0.38	Oral, blood	Observed
CL_T/F		19.6 L/h	-	35.1 L/h	-	0.56		Observed
CL_H/F		17.8 L/h	90.8%	30.49 L/h	86.8%	0.58		Calculated
CL_R	Ducharme et al. 1995	15.4 L/h	8.9 %	23.05 L/h	13.13%	0.66	Oral, plasma	Estimated
CL_T/F		168.6 L/h	-	175.5 L/h	-	0.96		Observed
CL_H/F		153.2 L/h	90.8 % T	152.45 L/h	86.8 %	1.00		Calculated

CL_R: renal clearance. CL_T: total clearance. CL_H: hepatic clearance. F: bioavailability

TABLE SIII - Predicted PK parameters of *R*-HCQ of *S*-HCQ in different CYP2C8 and CYP2D6 phenotypes

	(−)-R-HCQ		(+)-S-HCQ	
Phenotype	**AUC (ng/mL.h)**	**Cmax (ng/mL)**	**AUC (ng/mL.h)**	**Cmax (ng/mL)**
CYP2D6 NM	4202.5±1912.9 4031.47 (1718.5–7691.4)	99.8±26.1 99.6 (56.4–135.8)	1888.28±882 1827.7 (766.1–3342.9)	87.5±24.9 85.5 (46.5–124.4)
CYP2D6 PM	5305.7±2062.4 5130.4 (2540.1–8819.2)	104.3±24.1 105.4 (65.1–142.3)	2441.2±1016.8 2299 (1141.7–1440.8)	93.9±22.8 94.7 (57.2–130.3)
CYP2D6 UM	3780.8±1561 3608.6 (1634.5–6462.5)	99.3±24.6 98.6 (59.5–141.3)	1706.9±716.5 1576.1 (720.5–2927.5)	85.7±22.9 86.6 (50.4–124.1)
CYP2C8 NM	4202.5±1912.9 4031.4 (1718.5–7691.4)	99.8±26.1 99.6 (56.4–135.8)	4202.5±1912.9 4031.47 (1718.5–7691.4)	99.8±26.1 99.6 (56.4–135.8)
CYP2C8 PM	6553.4±1916.7 6550.7 (3503.7–9494.9)	107.9±24.4 108.1 (76.9–139.2)	3111.8±1016.9 3067.8 (1544.1–4725.6)	100.3±20.3 99.8 (70.7–130)
CYP2D6-CYP2C8 PM	8898.3±2242.3 8794.6 (5977.7–12416.7)	111.1±26.5 109.8 (76.2–153.2)	4487±1306.5 4368.6 (2771.8–6770.2)	106.6±25.6 104.8 (73.6–148.1)
CYP2C8 PM+ CYP3A4 inhibitor	7152.6±2147.7 7173.1 (3655.6–10563.4)	108.2±21.5 108.3 (77.1–140.6)	3388.5±1167.8 3399.5 (1559.5–5418.1)	100.8±20.5 100.1 (71.2–132.3)
CYP2D6-CYP2C8 PM + CYP3A4 inhibitor	9845.7±2439.2 9687.8 (6607.2–13839)	111.4±26.5 110.3 (76.3–153.2)	5064.9±1474.5 4952.6 (2939.7–7584.6)	107±25.7 105.1 (73.7–147.7)
CYP2D6-CYP2C8 NM + CYP3A4 inhibitor	4440.6±2061.5 4172.9 (1739.2–7934.3)	100.1±26.2 99.9 (57.1–136.7)	1975.4±932.9 1877.8 (751.1–3455.2)	88±25 86.1 (46.3–124.4)

Data presented as mean ± standard deviation; median (5^{th}–95^{th} percentiles). AUC: area under the curve. C_{max}: maximum concentration.